ISSN 0023-1584, Kinetics and Catalysis, 2010, Vol. 51, No. 6, pp. 898–906. © Pleiades Publishing, Ltd., 2010.
Original Russian Text © E.I. Nemykina, N.A. Pakhomov, V.V. Danilevich, V.A. Rogov, V.I. Zaikovskii, T.V. Larina, V.V. Molchanov, 2010, published in Kinetika i Kataliz, 2010, Vol. 51, No. 6, pp. 929–937.

YOUNG SCIENTISTS' SCHOOL

Effect of Chromium Content on the Properties of a Microspherical Alumina–Chromium Catalyst for Isobutane Dehydrogenation Prepared with the Use of a Centrifugal Thermal Activation Product of Gibbsite

E. I. Nemykina, N. A. Pakhomov, V. V. Danilevich, V. A. Rogov, V. I. Zaikovskii, T. V. Larina, and V. V. Molchanov

Boreskov Institute of Catalysis, Siberian Branch, Russian Academy of Sciences, Novosibirsk, 630090 Russia

e-mail: nemykina@catalysis.ru

Received December 15, 2009

Abstract—The states of chromium in both promoted and unpromoted alumina–chromium catalysts with various chromium contents prepared with the use of a centrifugal thermal activation product of gibbsite were studied in detail. The presence of five chromium species was found in the catalysts of this type: two Cr^{6+} and three Cr^{3+} species. The concentration of each particular chromium species depends on the total chromium content of the catalyst. Based on the experimental data, we hypothesized that highly disperse Cr^{3+} particles, the formation of which was completed at a chromium content of ~7–9 wt %, are responsible for the catalytic activity of alumina–chromium samples in the reaction of isobutane dehydrogenation.

DOI: 10.1134/S0023158410060169

INTRODUCTION

Dehydrogenation processes occupy an important place in the chemical industry. Unsaturated compounds, which are valuable materials as monomers for the manufacture of synthetic rubber and plastics and for the synthesis of high-octane gasoline components and other valuable chemical products, are produced by dehydrogenation. Currently, the Cr_2O_3/Al_2O_3 systems occupy more than a half of the world market of commercial catalysts for paraffin dehydrogenation or 100% of the domestic market in Russia. In this case, the following two types of alumina–chromium catalysts are used in industrial processes [1, 2]:

—granulated catalysts for a fixed-bed dehydrogenation process at a reduced partial pressure of a hydrocarbon (the Catofin process for the dehydrogenation of isobutane and propane and the Catadiene process for the single-step dehydrogenation of *n*-butane to butadiene);

—microspherical catalysts for a fluidized bed process for isobutane, isopentane, and propane dehydrogenation (the Yarsintez process).

In Russia, the major portion of olefins produced by dehydrogenation is manufactured using a fluidized-bed dehydrogenation process with an alumina–chromium catalyst. In this process, the catalyst circulates between a reactor and a regenerator and the heat of coke combustion is used to perform an endothermic dehydrogenation reaction [1]. The bottleneck of this technology is the low activity and high abradability of an IM-2201 alumina–chromium catalyst, which has been used for more than 30 years. In addition to a high consumption rate of this catalyst per ton of the resulting olefin, serious environmental problems occur in the course of its operation due to the trapping of catalyst microparticles formed in the course of its abrasion and the burial of a large amount of toxic spent catalysts [2, 3].

The AOK-73-21 catalyst has been introduced at some plants in 2000; this catalyst has been manufactured at ZAO Altailyuminofor (Yarovoe) until 2006. Although the mechanical strength and activity of this catalyst were higher than those of the IM-2201 catalyst, it has not found a wide application because of its inadequate hydrodynamic characteristics, high abrasive properties, and irreproducibility of the phase composition of the support—a flash product from the Achinsk Alumina Refinery [4]. It was found previously [5, 6] that the yield of isobutylene and selectivity in the reaction of isobutane dehydrogenation can be increased by 2–5 wt % on a new KDM catalyst, as compared with the AOK-73-21 catalyst, on going from a commercial flash product to a centrifugal thermal activation (CTA) product of gibbsite (hydrargillite) prepared in a TSEFLAR^{TM} centrifugal flash reactor with the retention of the other preparation parameters and catalyst composition.

The physicochemical properties of the CTA product of gibbsite and its rehydration to active aluminum hydroxides (pseudoboehmite and bayerite) have been studied in detail [7–9]. However, the formation of the

oxide compounds of chromium supported onto this product in the synthesis of a microspherical aluminum oxide catalyst for dehydrogenation has not been studied. In this work, which opens a series of publications concerning this system, we used a set of physicochemical techniques to study the state and catalytic properties of supported chromium oxide in the reaction of isobutane dehydrogenation depending on supported chromium content. A distinctive feature of this system from the extensively studied Cr_2O_3/Al_2O_3 catalysts [1, 10–12] is that active component precursors are supported onto an amorphous CTA product [8] rather than a preformed alumina oxide support. The CTA product exhibits high chemical activity, and it is readily hydrated to pseudoboehmite in an acidic medium in the presence of water. Thus, in the procedure used for preparing the catalyst, the stages of supporting an active component precursor and hydrating the CTA product are combined. Finally, the entire process of support formation occurs simultaneously with the formation of a supported active component.

EXPERIMENTAL

Preparation of the Support

The CTA product of gibbsite was prepared in a drum-type TSEFLAR™ apparatus at process parameters required for the synthesis of a product with a maximum concentration of an amorphous phase and, correspondingly, with a minimum concentration of undecomposed gibbsite impurities [8]. Gibbsite from the Achinsk Alumina Refinery was used as a starting raw material for thermal activation.

The resulting CTA product had the following characteristics:

—phase composition, 1.0 wt % gibbsite, 7.4 wt % boehmite, and 91.6 wt % amorphous phase;

—weight loss upon calcination at 800°C, 4.9 wt %;

—specific surface area, 230 m^2/g;

—pore volume (moisture capacity), 0.23 cm^3/g.

Before supporting an active component, a fraction of size smaller than 70 μm was sifted out from the CTA product.

Preparation of Catalyst Samples

The alumina–chromium catalysts were prepared by the incipient wetness impregnation of the CTA product using aqueous solutions of CrO_3 with various concentrations. The chromium content of the final catalyst was varied from 1 to 11.3 wt % in terms of Cr. The promoted samples were prepared by combined impregnation with aqueous solutions of CrO_3 containing potassium hydroxide and zirconium oxynitrate. The calculated concentrations of additives in the samples were 1.5 wt % K_2O and 1.0 wt % ZrO_2. In the preparation of an impregnating solution, the amount of water was taken 30% greater than that required for the incipient wetness impregnation of the support taking into account the fact that an excess water amount was consumed for the hydration on the CTA product. The impregnation was performed for 1 h at room temperature with continuous stirring in a Z-shaped mixer. Thereafter, the samples were dried in air at room temperature until a free-flowing state and then in a drying oven at 120°C for 4 h. The dried samples were calcined in air at 700°C in a muffle furnace for 1 h.

Physicochemical Investigation Techniques

To determine the total chromium content of the catalysts, the samples were precalcined at 700°C to remove adsorbed water and then completely dissolved in concentrated sulfuric acid. The concentration of soluble Cr^{6+} species was determined by boiling a weighed portion of the catalyst in water. The solutions were analyzed by inductively coupled plasma atomic emission spectrometry (ICP AES) on an Optima 4300 DV instrument.

The total concentration of Cr^{6+} ions was determined by the temperature-programmed reduction (TPR) of calcined samples in a flow setup with a thermal-conductivity detector. Before the reduction, the samples were trained in oxygen for 0.5 h at 500°C. The samples after boiling in water were trained in argon for 0.5 h at 150°C in order to prevent the repeated formation of a soluble Cr^{6+} species in the presence of oxygen. After training, the samples were cooled to room temperature and blown with argon. The sample weight was 100–200 mg; the supply rate of a reducing mixture (10% hydrogen in argon) was 40 cm^3/min; the heating rate was 10 K/min.

The phase compositions of the supports and catalysts were determined by X-ray diffraction (XRD) analysis. The XRD patterns of the test samples were measured on an HGG 4-C diffractometer using monochromated CuK_α radiation (a flat graphite monochromator in the diffracted beam) over the angle range of 10°–70° (2θ) by point-by-point scanning. The scanning step was 0.05°, and the accumulation time at a point was 5 s.

The high-resolution transmission electron-microscopic (HR TEM) images were obtained on a JEM-2010 electron microscope (JEOL, Japan) with a lattice resolution of 0.14 nm at an accelerating voltage of 200 keV. Energy dispersive X-ray (EDX) analysis was performed on an EDAX spectrometer (EDAX) equipped with a Si(Li) detector with an energy resolution of 130 eV. The test samples were fixed on standard copper gauzes, which were placed in a holder and introduced into the sample chamber of the electron microscope.

The electronic diffuse reflectance spectra in the UV and visible regions were taken on a UV-2501 PC spec-

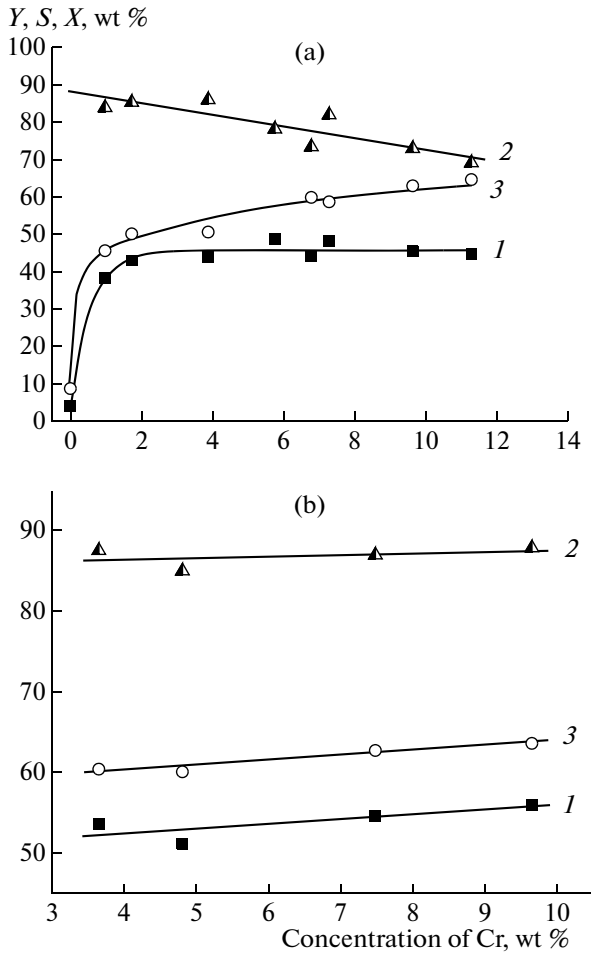

Fig. 1. Dependence of (*1*) the yield of isobutylene (*Y*), (*2*) selectivity for isobutylene (*S*), and (*3*) isobutane conversion (*X*) in the isobutane dehydrogenation reaction on the concentration of chromium in (a) unpromoted Cr_2O_3/Al_2O_3 samples and (b) samples containing 1.5% K_2O and 1.0% ZrO_2.

trophotometer from Shimadzu with an ISR-240A diffuse reflectance attachment. The samples as 100-μm granules were placed in a quartz cell with an optical path length of 2 mm. The spectra were measured with reference to a $BaSO_4$ reflection standard substance over the range of 11000–54000 cm^{-1}. The electronic diffuse reflectance spectroscopic data were presented in the Kubelka–Munk function–wavenumber coordinates.

The adsorption studies were performed using N_2 adsorption isotherms at 77 K, which were measured on an ASAP-2400 instrument (Micromeritics, United States) after training the samples in a vacuum at 150°C. The isotherms were used to calculate the total accessible surface area by the BET method and the total pore volume (V_Σ) with effective sizes to 100–200 nm (based on adsorption at a relative nitrogen pressure of 0.99).

Catalytic Tests

The catalytic activity of the samples was studied in the reaction of isobutene dehydrogenation in a fluidized bed of a catalyst. The experiments were performed on an automated laboratory bench. The process was performed in short (10 min) dehydrogenation experiments at 580°C followed by catalyst regeneration to remove carbon deposits at 650°C using an air–nitrogen mixture (50 : 50, by volume). The feed space velocity was 400 h^{-1}.

The initial gases and reaction products were analyzed on a Khromos GKh-1000 chromatograph with a flame-ionization detector (FID) and 30-m SiO_2 capillary column. The test sample was taken from a gas flow by automatically turning sampling valves using pneumatic actuators with solenoid valves. The results of analysis were displayed on a computer and calculated using the Khromos special software by the internal standard method. In special experiments, it was found that catalytic characteristics remained almost unchanged within the limits of experimental error over a reaction time interval from 5 to 12–15 min. For this reason, catalysts were compared based on the results of the analysis of a sample taken 10 min after the onset of reaction.

RESULTS AND DISCUSSION

Catalytic properties. Figure 1a shows the dependence of catalytic characteristics in the reaction of isobutane dehydrogenation on the concentration of chromium in Cr_2O_3/Al_2O_3 samples with no promoting additives. In Fig. 1a, it can be seen that, as the concentration of chromium was increased from 0 to 1 wt %, a dramatic increase in the yield of isobutylene and the degree of isobutane conversion was observed. As the concentration of chromium was further increased to 11–12 wt %, the yield of isobutylene did almost not increase. In this case, the observed increase in conversion was accompanied by a decrease in the process selectivity because of an increase in the fraction of cracking products. Note that the samples with no modifying additives were much worse than commercial catalysts in terms of catalytic characteristics.

Figure 1b illustrates data on the dependence of catalytic characteristics in the isobutane dehydrogenation reaction on the chromium content of promoted samples. As expected, the introduction of additives considerably increased the catalytic characteristics. In this case, note that, at low chromium concentrations in the catalyst (3.5–4.5 wt %), the yield of isobutylene was 52–54 wt % at a selectivity of 85–87 wt %. An almost threefold increase in the concentration of chromium to a level of chromium concentrations in AOK-73-21 and KDM commercial catalysts [7] (14–16 wt % in terms of Cr_2O_3) resulted in an increase in the yield of isobutylene and in the selectivity by only 2–3 wt %. In this context, two questions arose: why is

the regulated chromium content of commercial catalysts so high and whether the use of the CTA product as a starting support is a prerequisite to decrease the chromium content of the catalysts? An analysis of data given in Fig. 1b indicates that a decrease in the chromium content of the catalyst to 7–8 wt % Cr (10.5–12.0 wt % Cr_2O_3) makes it possible to obtain expedient performance characteristics in the isobutane dehydrogenation reaction. High catalytic activity and selectivity at the given chromium concentrations were also reached at lower dehydrogenation temperatures. Thus, the yield of isobutylene at 560°C was 50–51 wt % at a selectivity of 93 wt %; these values compare well with the values reached on a KDM commercial catalyst [7]. Thus, based on the results of the laboratory tests of the average samples of the KDM catalyst from various commercial batches, the yield of isobutylene was 48–50 wt % at a selectivity of 92–93 wt %. In this case, the chromium content of these samples was 11 wt %.

To determine the nature of an active component and to explain the found dependence of catalytic characteristics on the concentration of chromium, we studied unpromoted and promoted samples using a set of physicochemical techniques.

XRD data and texture characteristics. Figure 2 shows the XRD patterns of unpromoted Cr_2O_3/Al_2O_3 samples with various chromium concentrations. For comparison, Fig. 2 (curve *1*) shows the XRD pattern of the starting CTA product calcined at the same temperature as the calcination temperature of the samples. An analysis of the XRD patterns indicates that, in a range of chromium concentrations from 0 to 10 wt %, the XRD patterns exhibited only diffraction peaks due to the γ-Al_2O_3 support; in this case, the intensity of lines attributed to this phase decreased with chromium concentration. In addition to the γ-Al_2O_3 phase, the support contained trace amounts (no more than 5 wt %) of a χ-Al_2O_3 phase. The most intense lines of a crystalline α-Cr_2O_3 phase (at $2\theta = 24.5°$ (24.7°), 33.7° (34.1°), 36.4°, 41.5°, and 54.7° (55.4°) [13]) were detected only in the XRD pattern of a sample with a maximum chromium content of 11.3 wt %. In this case, note that the experimental positions of lines due to the chromium oxide phase (the values given in parentheses) were shifted toward greater angles, as compared with tabulated values [14]; this suggests the formation of a crystalline solid solution phase based on α-Cr_2O_3. According to published data [15], the formation of the α-Cr_2O_3 phase began at a chromium concentration of ~8 wt % in the Cr_2O_3/Al_2O_3 sample with a support specific surface area of 80 m^2/g. At the same time, note that the diffraction peaks of the support shifted to the region of smaller angles with increasing chromium content. The table summarizes the lattice parameters calculated for the cubic structure of aluminum oxide. As the chromium content was increased, the lattice parameter of the support increased from 0.7908 nm for the chromium-free CTA sample to 0.7974 nm for the sample containing 11.3 wt % chromium. An increase in the lattice parameter of the support was also observed in promoted samples. As explained by Moroz et al. [16], the lattice parameter increased due to the insertion of Cr^{3+} ions into the support structure and the formation of a Cr_2O_3–γ-Al_2O_3 solid solution. Consequently, the fraction of Cr^{3+} ions dissolved in the support increased with the chromium content of the catalyst.

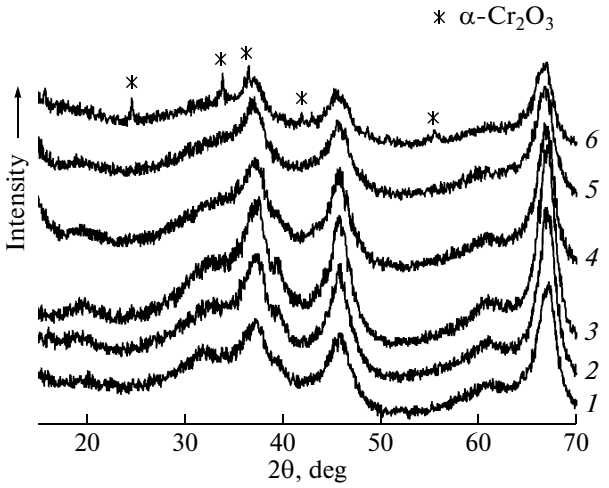

Fig. 2. X-ray diffraction patterns of unpromoted Cr_2O_3/Al_2O_3 samples with the following chromium concentrations, wt %: (*1*) 0, (*2*) 1.0, (*3*) 1.7, (*4*) 6.8, (*5*) 9.7, and (*6*) 11.3.

According to adsorption data in unpromoted samples, the specific surface area of the catalyst decreased with increasing chromium content to 6 wt % or higher; simultaneously, the pore volume decreased (see the table). Because, according to XRD data, the particle size (CSR) of the support in the catalyst did not change considerably in this case, the symbatic decrease of the pore surface area and the pore volume can be explained by the fact that small pores were blocked by chromium oxide particles. These results suggest that, in addition to the dissolution of a portion of Cr^{3+} ions in the support, the formation of dispersed chromium oxide particles came into play at a chromium content of the catalyst higher than 6 wt %. As can be seen in the table, a tendency toward decreasing the specific surface area and volume of pores with increasing chromium content was retained upon the introduction of promoting additives (potassium and zirconium oxides) into the catalyst. At high chromium contents, these values for promoted samples were lower than those for unpromoted ones.

HR TEM data. According to electron-microscopic data, both promoted and unpromoted samples with chromium concentrations lower than 8 wt % consisted of γ-Al_2O_3 aggregates with a defect (microblock) spinel structure, which are pseudomorphous with respect to the starting hydroxide (Fig. 3a). The sizes of

Changes in structure and texture characteristics depending on the concentration of chromium in the unpromoted and promoted samples of a microspherical Cr_2O_3/Al_2O_3 catalyst

Concentration of Cr, wt %	Support lattice parameter, nm	CSR, nm	Specific surface area, m^2/g	Pore volume, cm^3/g
0	0.7908	6.0	119	0.18
No promoters				
1.0	0.7933	5.8	117	0.17
1.7	0.7933	–	119	0.17
6.8	0.7941	6.0	102	0.14
9.7	0.7949	–	90	0.13
11.3	0.7974	5.9	81	0.12
K_2O (1.5 wt %) and ZrO_2 (1.0 wt %) promoters				
3.7	0.7933	6.0	97	0.15
4.8	–	–	113	0.15
7.5	0.7916	6.0	98	0.14
9.5	0.7941	8.0	75	0.11

the aggregates were 200 nm or greater; they consisted of blocks (primary crystallites) of size 5–10 nm separated by disordered mesopores (~5 nm). The electron microdiffraction patterns obtained from these aggregates contained a two-dimensional network of point reflections having the azimuthal broadening $\Delta\varphi$ of no higher than 3°, corresponding to the disorientation of primary Al_2O_3 crystallites (Fig. 3). Note that a small portion of dispersed γ-Al_2O_3 crystallites occurred in an isolated form.

The crystalline particles of chromium oxide were not detected in these samples by TEM. However, the EDX spectra from γ-Al_2O_3 particles contained signals due to both Al and Cr with the ratio Al : Cr ≈ 85 : 15 and signals from the K and Zr promoter elements (Fig. 3c). This result supports XRD data on the dissolution of chromium ions in the support.

The EDX spectra from pseudomorphous γ-Al_2O_3 aggregates in the sample containing 11.3 wt % Cr also exhibited the formation of a solid solution of Cr ions in γ-Al_2O_3 (Al : Cr ≈ 75 : 25). However, in addition, the formation of a second phase as individual large crystals of size 100 nm or greater was observed (Fig. 3c). According to XRD data, large crystals of this size correspond to the phase of a solid solution of Al in α-Cr_2O_3. The EDX spectra (Fig. 3e) also exhibited the formation of a solid solution of Al in α-Cr_2O_3 with the atomic ratio Al : Cr ≈ 15 : 85. Thus, as the chromium content of the catalyst was increased, the complete dissolution of chromium ions in aluminum oxide did not occur; therefore, an excess of chromium crystallized as a solid solution based on α-Cr_2O_3.

Electronic diffuse reflectance spectroscopic data. The states of chromium in a promoted sample containing 7.5 wt % Cr were studied by electronic diffuse reflectance spectroscopy. In Fig. 4, curve *1* belongs to an initial sample calcined at 700°C in air. From published data [17, 18], it follows that an absorption band (16600 cm^{-1}) and shoulders (14200 and 22800 cm^{-1}) in the visible region of the electronic diffuse reflectance spectrum were due to *d–d* transitions characteristic of Cr^{3+} cations in an octahedral oxygen coordination, whereas absorption bands in the UV region of the spectrum were due to ligand–ligand charge transfer characteristic of Cr^{6+} cations in an octahedral oxygen coordination.

Figure 4 (curve *2*) shows the spectrum of a sample after boiling in water and drying in air at room temperature. A comparison between the electronic diffuse reflectance spectra of the initial sample and the sample after boiling indicates that the same three absorption bands at 16600, 27000, and 35900 cm^{-1} and shoulders at 14200 and 22800 cm^{-1} were observed in both of the samples. Hence, it follows that the above two states of chromium (Cr^{6+} and Cr^{3+}) were retained in the sample after boiling.

Figure 4 (curve *3*) shows the spectrum of the initial sample after reduction in an atmosphere of hydrogen. For the correct interpretation of this spectrum, Fig. 4 also shows the spectrum of bulk α-Cr_2O_3 (curve *4*). The visible region of this spectrum exhibited symmetric absorption bands at 16600 and 21600 cm^{-1} due to *d–d* transitions in Cr^{3+} cations having an octahedral oxygen coordination and absorption bands in the UV region of the spectrum at 28600 and 34500 cm^{-1} due to ligand–metal charge transfer in Cr^{3+} complexes having an octahedral oxygen coordination. Hence, it follows that the absorption bands at 16600 and 22800 cm^{-1} in the reduced catalyst (curve *3*) can also be due to *d–d* transitions in Cr^{3+} cations in α-Cr_2O_3. However, a shift of the center of an absorption band at 22800 cm^{-1} in the electronic diffuse reflectance spectrum of an alumina–chromium sample after its reduction in an atmosphere of hydrogen with respect to the absorption band at 21600 cm^{-1} for bulk α-Cr_2O_3 suggests the stabilization of a portion of Cr^{3+} cations in

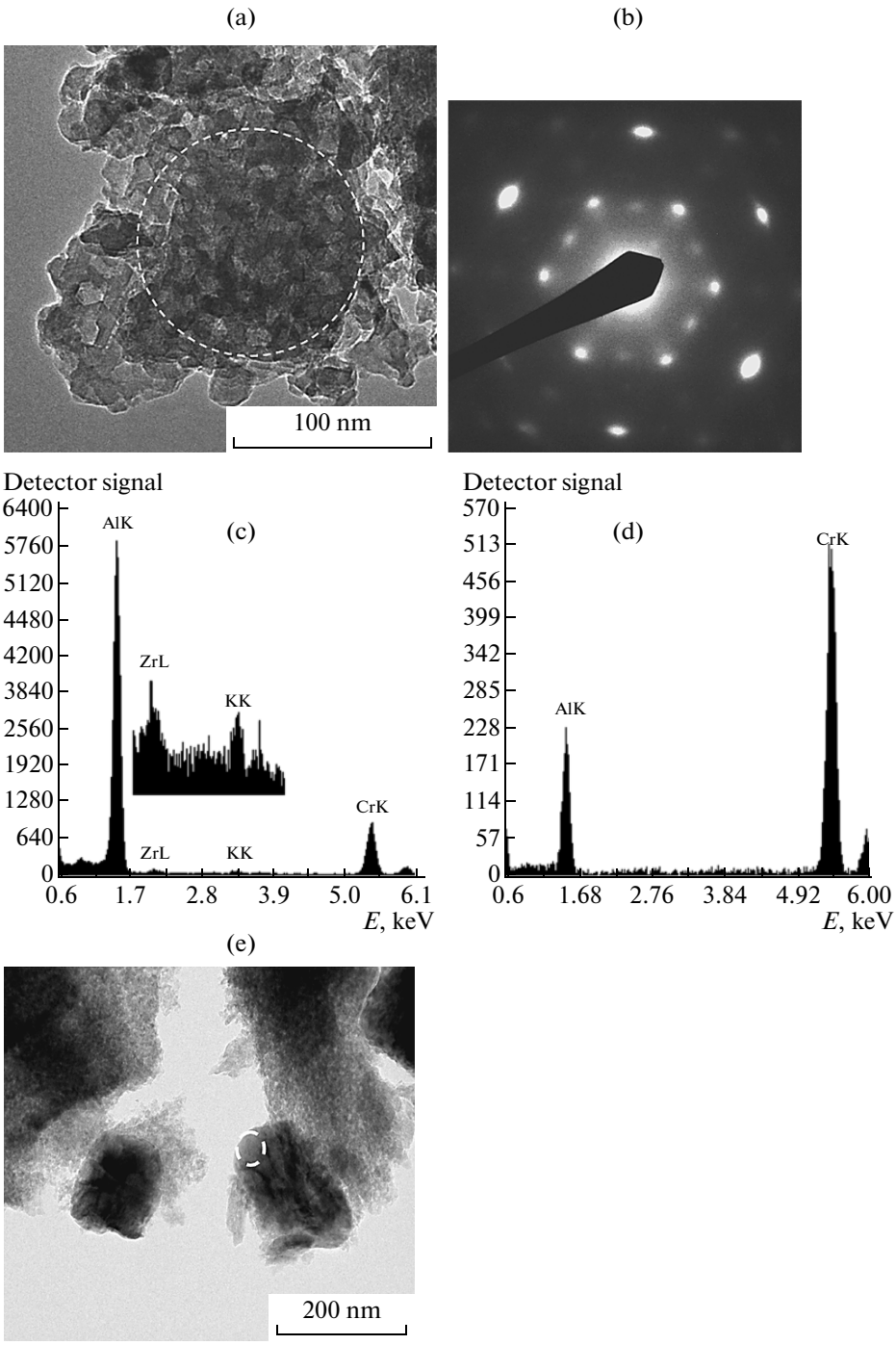

Fig. 3. Sample characterization by TEM and EDX: (a) TEM image of a γ-Al_2O_3 aggregate in a promoted sample containing 7.5 wt % Cr (the circle marks a region for microdiffraction and X-ray microanalysis); (b) electron microdiffraction from the aggregate; (c) EDX spectrum from a γ-Al_2O_3 aggregate (Fig. 3a) with the signals of Al, Cr, K, and Zr (the insert shows a magnified region of the spectrum); (d) coarse crystalline particles of a solid solution of Al in α-Cr_2O_3 contacting with Al_2O_3 in a sample containing 11.3 wt % Cr (the circle marks a region for X-ray microanalysis) (e) EDX spectrum from a particle region (Fig. 3d) of the solid solution of Al in α-Cr_2O_3 in a sample containing 11.3 wt % Cr.

the cationic vacancies of γ-Al_2O_3. A dramatic decrease in the intensity of an absorption band at 28600 cm^{-1} for the alumina–chromium sample reduced in an atmosphere of hydrogen with reference to its pair at 34500 cm^{-1} for bulk α-Cr_2O_3 (curve *4*) also suggests the insertion of a portion of Cr^{3+} cations into the γ-Al_2O_3 support. A comparison of all of the electronic diffuse reflectance spectra indicates that a broad symmetric absorption band at 37700 cm^{-1}, which occurred in the electronic diffuse reflectance spectra

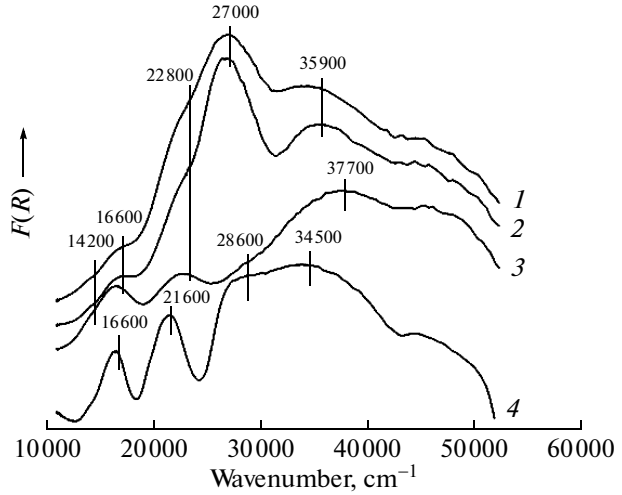

Fig. 4. Diffuse reflectance spectra of a Cr_2O_3/Al_2O_3 sample containing 7.5 wt % chromium after various treatments: (*1*) initial sample, (*2*) after boiling and drying at 20°C, (*3*) after reduction in an atmosphere of hydrogen, and (*4*) bulk α-Cr_2O_3.

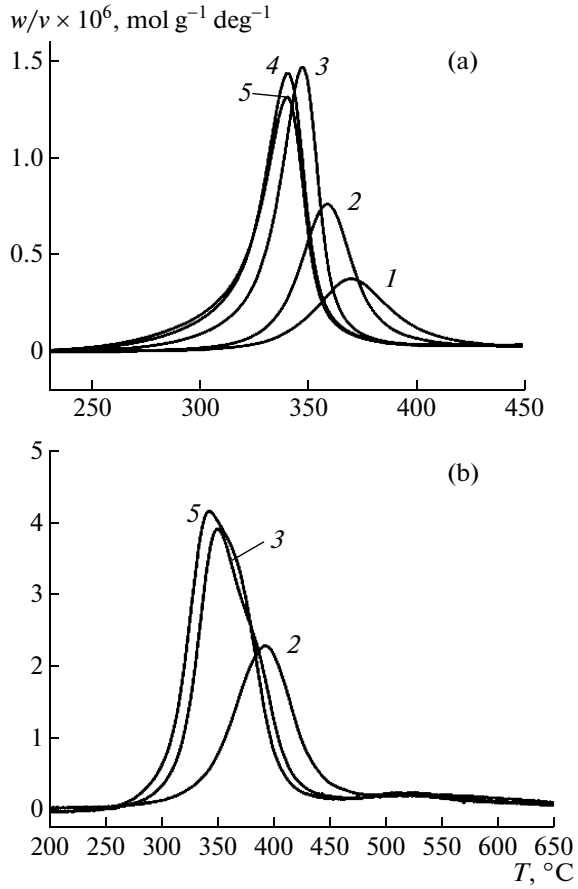

Fig. 5. TPR spectra of Cr_2O_3/Al_2O_3 samples: (a) initial and (b) after boiling in water and drying in a flow of argon. Chromium concentrations, wt %: (*1*) 1.0, (*2*) 1.7, (*3*) 6.8, (*4*) 9.7, and (*5*) 11.3. The rate of hydrogen consumption (w, mol g^{-1} s^{-1}) referred to the rate of heating (v, K/s) is plotted on the Y axis.

of almost all of the alumina–chromium samples, was most likely due to the stabilization of a portion of Cr^{3+} cations in the cationic vacancies of γ-Al_2O_3.

TPR data. Because the concentrations of the above chromium species, including Cr^{6+} ions, cannot be determined quantitatively by electronic diffuse reflectance spectroscopy, we proposed a combined procedure for the quantitative determination of these species using TPR and spectroscopic chemical analysis.

Figure 5 shows the TPR spectra of the initial samples with no modifying additives and the samples after boiling (containing no soluble Cr^{6+} ions). The total concentration of Cr^{6+} ions in the catalysts was calculated from the total consumption of H_2 in the temperature range of 200–500°C and according to published data [19] on the stoichiometry of the reaction $2CrO_3 + 3H_2 = Cr_2O_3 + 3H_2O$. In Fig. 5a, it can be seen that an increase in the concentration of Cr^{6+} was observed as the total chromium content of the samples was increased to 6.8 wt %; the amount of Cr^{6+} remained unchanged as the chromium content was further increased.

Figure 6a shows the concentrations of various chromium species according to TPR and chemical analysis data for unpromoted samples with various chromium contents.

An analysis of the above data allowed us to conclude that at least two types of chromium oxides in the oxidation state of Cr^{6+} were present in the calcined samples of the microspherical catalyst:

—weakly grafted water-soluble Cr^{6+} oxides and

—water-insoluble Cr^{6+} ions, which can be strongly grafted to the support surface.

Data given in Fig. 6a indicate that the concentrations of both of the Cr^{6+} ionic species dramatically increased as the total concentration of chromium was increased to 2–4 wt % and then flattened out. In this case, the amount of the soluble species was smaller than that of the strongly grafted species.

The fraction of Cr^{3+} ions in the catalyst determined by difference between the total chromium concentration and the total concentration of Cr^{6+} ions became higher than the amount of Cr^{6+} ions at a chromium concentration higher than 3 wt %. These data are consistent with published data [15].

Figure 6b shows the dependence of the concentrations of various chromium species on the total concentration of chromium in samples with promoting additives.

Comparing data in Figs. 6a and 6b, we can note that they are qualitatively similar: starting with 4 wt % Cr, the concentration of all types of Cr^{6+} ions remained almost constant. However, on closer examination, we can recognize two main differences between promoted and unpromoted samples:

—an increase in the total concentration of Cr^{6+} ions from 1.8 wt % in samples with no promoters to 2.0–2.2 wt % in samples with promoters;

—an increase in the amount of soluble chromium oxide species in the oxidation state Cr^{6+} because of the additional formation of potassium chromates with a simultaneous decrease in strongly grafted Cr^{6+} ions.

Because, according to data in Fig. 1a, catalytic characteristics in the isobutane dehydrogenation reaction were considerably enhanced upon the introduction of promoting additives, we can assume that Cr^{3+} ions formed upon the reduction of soluble Cr^{6+} species under the action of a reaction atmosphere were most active and selective since the amount of these ions increased upon the introduction of the additives.

States of supported chromium oxide and their role in dehydrogenation. Summarizing data obtained by all of the investigation techniques used, we can state that chromium occurred in five different states in alumina–chromium catalysts prepared by the CTA product—gibbsite. Among them are two Cr^{6+} species (soluble and grafted) and three Cr^{3+} species (as a solid solution in the support lattice, highly dispersed α-Cr_2O_3 particles on the catalyst surface, and coarse α-Cr_2O_3 particles on the catalyst surface).

The question of what is the active center of alumina–chromium catalysts in dehydrogenation reactions is still an open question in the literature. In earlier studies, Cr^{2+} ions were considered as active sites [20, 21]. More recently, the majority of researchers concluded that Cr^{3+} ions were responsible for activity [1, 22–24]. In this case, some of them hold to the idea that coordinatively unsaturated Cr^{3+} ions exhibited catalytic activity [1, 24].

In our opinion, the main active states are highly dispersed chromium oxide particles in the oxidation state Cr^{3+}. However, we can see that, at a low concentration of chromium when Cr^{3+} particles were almost absent from the calcined catalyst and chromium almost entirely occurred as Cr^{6+}, the catalyst also exhibited a sufficiently high catalytic activity. Consequently, the reduction of Cr^{6+} led to the formation of active sites. In this case, in our opinion, Cr^{3+} particles formed upon the reduction of soluble Cr^{6+} species were more active and selective. This conclusion follows from the fact that a considerable increase in catalytic characteristics in the isobutane dehydrogenation reaction was observed upon the introduction of promoting additives. In this case, the amount of soluble Cr^{6+} increased and the amount of grafted Cr^{6+} decreased.

To support this hypothesis, we performed an additional experiment. An unpromoted sample containing 6.8 wt % Cr was boiled for an hour to remove a soluble Cr^{6+} phase. In this case, the total concentration of chromium in the sample decreased to 6.2 wt %. Thereafter, the sample was initially dried and then heated to a catalytic experiment temperature of 580°C in a flow of helium in order to avoid the reoxidation of the sample. According to the results of catalytic tests, the yield of isobutylene after boiling decreased by 10 wt % and the selectivity decreased by 15 wt %, as compared with the initial sample at an unchanged degree of conversion. Based on these data, we can conclude that the phase of soluble Cr^{6+}, although its concentration was relatively low (no higher than 1 wt % Cr), afforded highly active and selective dehydrogenation sites upon reduction under reaction conditions. On the other hand, this experiment supported the fact that sites from a phase of Cr^{3+} present in the initial catalyst were also responsible for catalytic activity. However, it is likely that they were less active and selective.

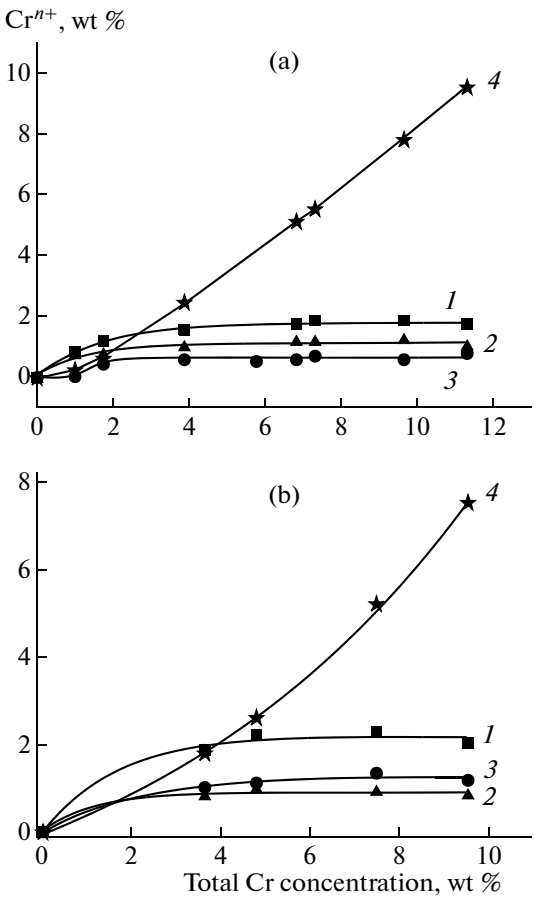

Fig. 6. Dependence of the concentrations of (*1*) total Cr^{6+}, (*2*) grafted Cr^{6+}, (*3*) soluble Cr^{6+}, and (*4*) Cr^{3+} on the total chromium content of (a) unpromoted and (b) promoted Cr_2O_3/Al_2O_3 samples.

The coarse crystals of α-Cr_2O_3 were inactive in the dehydrogenation reaction. The major portion of Cr^{3+} ions that formed a solid solution with the support did not participate in the dehydrogenation reaction. However, they can play a certain role in the stabilization of the support structure upon calcination.

The formation of chromium particles in the form of Cr^{6+} was complete at a chromium content of about 4–

5 wt %. A further increase in the chromium content resulted in an increase in the Cr^{3+} content. It is likely that chromium dissolution in the support and the formation of highly dispersed Cr_2O_3 particles on the catalyst surface occurred simultaneously in this case. The dissolution of Cr^{3+} ions in the support was the main reason for the very slow growth of catalyst activity (Fig. 1) over a wide range of chromium concentrations. The upper limit of optimum chromium concentrations in the catalyst was determined by the onset of the intense formation of coarsely crystalline inactive α-Cr_2O_3 particles. This limit is very diffuse; in principle, this fact allowed us to conclude that the chromium content of commercial catalysts prepared with the use of the CTA product can be decreased to 8 wt %.

REFERENCES

1. Weckhuysen, B.M. and Schoonheydt, R.A., *Catal. Today*, 1999, vol. 51, p. 223.
2. Pakhomov, N.A., in *Promyshlennyi kataliz v lektsiyakh* (Industrial Catalysis: Lectures), Moscow: Kalvis, 2005, issue 6, p. 87.
3. Nikolaev, V.V., Busygina, N.V., and Busygin, I.G., *Osnovnye protsessy fizicheskoi i fiziko-khimicheskoi pererabotki gaza* (Basic Processes in the Physical and Physicochemical Processing of Natural Gas), Moscow: Nedra, 1996, p. 273.
4. Kotelnikov, G.R., *React. Kinet. Catal. Lett.*, 1995, vol. 55, no. 2, p. 537.
5. Sanfilippo, D., Buonomo, F., Fusco, G., Lapieri, M., and Miracca, I., *Chem. Eng. Sci.*, 1992, vol. 47, nos. 9–11, p. 2313.
6. Taraban, E.A. and Simagina, V.I., *Katal. Prom–sti.*, 2002, no. 4, p. 14.
7. Pakhomov, N.A., Molchanov, V.V, Zolotovskii, B.P., Nadtochii, V.I., Isupova, L.A., Tikhov, S.F., Kashkin, V.N., Kharina, I.V., Balashov, V.A., Tanashev, Yu.Yu., and Parakhin, O.A., *Katal. Prom–sti.*, 2008, special issue, p. 13.
8. RF Patent 2322290, 2002.
9. Kharina, I.V., Isupova, L.A., Litvak, G.S., Moroz, E.M., Kryukova, G.N., Rudina, N.A., Tanashev, Yu.Yu., and Parmon, V.N., *Kinet. Katal.*, 2007, vol. 48, no. 2, p. 343 [*Kinet. Catal.* (Engl. Transl.), vol. 48, no. 2, p. 327].
10. Isupova, L.A., Tanashev, Yu.Yu., Kharina, I.V., et al., *Chem. Eng. J.*, 2005, vol. 107, nos. 1–3, p. 163.
11. Tanashev, Yu.Yu., Moroz, E.M., Isupova, L.A., Ivanova, A.S., Litvak, G.S., Amosov, Yu.I., Rudina, N.A., Shmakova, A.N., Stepanov, A.G., Kharina, I.V., Kul'ko, E.V., Danilevich, V.V., Balashov, V.A., Kruglyakov, V.Yu., Zolotarskii, I.A., and Parmon, V.N., *Kinet. Katal.*, 2007, vol. 48, no. 1, p. 161 [*Kinet. Catal.* (Engl. Transl.), vol. 48, no. 1, p. 153].
12. Poole, Ch., MacIver D, *Adv. Catal.*, 1967, no. 17, p. 224.
13. Vuurman, M., Hardcastle, F., and Wachs, E., *J. Mol. Catal.*, 1993, no. 46, p. 193.
14. ICDD PDF 2 00-029-0063.
15. Cavani, F., Koutyrev, M., Trifiro, F., Bartolini, A., Ghisletti, D., Iezzi, R., Santucci, A., and Del Piero, G., *J. Catal.*, 1996, no. 158, p. 236.
16. Moroz, E. Kirichenko, O., Ushakov, A.V., and Levitskii, E.A., *React. Kinet. Catal. Lett.*, 1985, vol. 28, no. 1, p. 9.
17. Snytnikov, V.N., Stoyanovskii, V.O., Larina, T.V., Krivoruchko, O.P., Ushakov, V.A., and Parmon, V.N., *Kinet. Katal.*, 2008, vol. 49, no. 2, p. 307 [*Kinet. Catal.* (Engl. Transl.), vol. 49, no. 2, p. 291].
18. Lever, A.B.P., *Inorganic Electronic Spectroscopy*, Amsterdam: Elsevier, 1987, p. 443.
19. Gaspar, A. and Dieguez, L., *J. Catal.*, 2003, vol. 220, no. 2, p. 309.
20. Ashmawy, F., *J. Chem. Soc., Faraday Trans. 1*, 1980, no. 76, p. 2096.
21. Slovetskaya, K.I. and Rubinshtein, A.M., *Kinet. Katal.*, 1968, vol. 8, no. 5, p. 115.
22. Marcilly, Ch. and Delmon, B., *J. Catal.*, 1972, no. 24, p. 336.
23. Shvets, V.A. and Kazanskii, V.B., *Kinet. Katal.*, 1966, vol. 7, no. 4, p. 712.
24. De Rossi, S., Ferraris, G., Fremiotti, S., Cimino, A., and Indovina, V., *Appl. Catal., A,* 1992, no. 81, p. 113.